

Article

Unraveling the chemical state of Cobalt in Co-based catalysts during Ethanol Steam Reforming: an *in situ* study by Near Ambient Pressure XPS and XANES

Cristian Huck-Iriart, Lluís Soler, Albert Casanovas, Carlo Marini, Jordi Prat, Jordi Llorca, and Carlos Escudero

ACS Catal., Just Accepted Manuscript • DOI: 10.1021/acscatal.8b02666 • Publication Date (Web): 06 Sep 2018

Downloaded from <http://pubs.acs.org> on September 7, 2018

Just Accepted

“Just Accepted” manuscripts have been peer-reviewed and accepted for publication. They are posted online prior to technical editing, formatting for publication and author proofing. The American Chemical Society provides “Just Accepted” as a service to the research community to expedite the dissemination of scientific material as soon as possible after acceptance. “Just Accepted” manuscripts appear in full in PDF format accompanied by an HTML abstract. “Just Accepted” manuscripts have been fully peer reviewed, but should not be considered the official version of record. They are citable by the Digital Object Identifier (DOI®). “Just Accepted” is an optional service offered to authors. Therefore, the “Just Accepted” Web site may not include all articles that will be published in the journal. After a manuscript is technically edited and formatted, it will be removed from the “Just Accepted” Web site and published as an ASAP article. Note that technical editing may introduce minor changes to the manuscript text and/or graphics which could affect content, and all legal disclaimers and ethical guidelines that apply to the journal pertain. ACS cannot be held responsible for errors or consequences arising from the use of information contained in these “Just Accepted” manuscripts.

1
2
3
4
5
6
7 Unraveling the chemical state of Cobalt in Co-
8
9
10 based catalysts during Ethanol Steam Reforming:
11
12
13
14
15 an *in situ* study by Near Ambient Pressure XPS
16
17
18
19 and XANES
20
21
22
23

24 *Cristián Huck-Iriart*^{1,2}, *Lluís Soler*³, *Albert Casanovas*³, *Carlo Marini*¹, *Jordi Prat*¹, *Jordi*
25
26 *Llorca*^{3,*}, *Carlos Escudero*^{1,*}
27
28
29

30 ¹ALBA Synchrotron Light Source, Carrer de la Llum 2–26, 08290 Cerdanyola del Vallès,
31
32 Barcelona (Spain)
33
34

35 ²Escuela de Ciencia y Tecnología, Universidad Nacional de San Martín (UNSAM),
36
37 Campus Miguelete, 25 de Mayo y Francia, 1650 San Martín, Provincia de Buenos Aires
38
39 (Argentina)
40
41
42

43 ³Institute of Energy Technologies, Department of Chemical Engineering and Barcelona
44
45 Research Center in Multiscale Science and Engineering, Universitat Politècnica de
46
47 Catalunya, EEBE, Eduard Maristany 10-14, 08019 Barcelona, (Spain)
48
49
50

51 *Corresponding authors. E-mails: jordi.llorca@upc.edu, cescudero@cells.es
52
53
54
55
56
57
58
59
60

1
2
3 Keywords: cobalt talc, cobalt hydrotalcite, cobalt spinel, ethanol steam reforming, *in situ*
4 spectroscopy, NAP-XPS, XANES
5
6
7
8
9
10

11 ABSTRACT

12
13
14
15 The steam reforming of ethanol (ESR) has been studied by Near Ambient Pressure XPS
16 (NAP-XPS), Extended X-ray Absorption Fine Structure (EXAFS) and X-ray Absorption
17 Near Edge Structure (XANES) under *in situ* conditions in the ALBA synchrotron facility at
18 200-580°C and S/C=3 over different cobalt-based catalysts that showed different catalytic
19 performance: $\text{Co}_3[\text{Si}_2\text{O}_5]_2(\text{OH})_2$ (Co-talc), $[\text{Co}_2\text{Mg}_4\text{Al}_2(\text{OH})_{16}]\text{CO}_3 \cdot 4\text{H}_2\text{O}$ (Co-hydrotalcite
20 shortened as Co-HT) calcined at 550°C, and Co_3O_4 (Co-spinel). Both, Co-spinel and Co-
21 talc yield to a greater or lesser degree metallic cobalt under ESR conditions. While the Co-
22 spinel shows a complete reduction to metallic cobalt under the conditions used for the
23 XANES measurements, more bulk-sensitive, the Co-talc sample exhibits only a partial
24 reduction. On the other hand under the ESR conditions used with the NAP-XPS, a more
25 surface sensitive technique, the results indicate a higher reduction degree for the Co-talc
26 sample as compared to the Co-spinel. In contrast, the catalyst prepared from the Co-HT
27 does not show metallic cobalt traces under the experimental conditions used with both
28 techniques. Comparing these three cobalt-based catalysts, the stable operation exhibited by
29 Co-HT under ESR reaction conditions is justified by the absence of metallic cobalt
30 formation under *in situ* conditions, which is identified as responsible for the carbon
31 deposition phenomena that triggers the deactivation suffered by most cobalt-based catalysts
32 during ESR.
33
34
35
36
37
38
39
40
41
42
43
44
45
46
47
48
49
50
51
52
53
54
55
56
57
58
59
60

1. INTRODUCTION

The steam reforming of ethanol (ESR) is a well-known process used for generating hydrogen (eq. 1). It is particularly interesting for the on-site and on-board production of hydrogen due to the widespread use of ethanol and its safe transport and storage^{1,2}. The steam reforming of renewable bioethanol (ethanol produced from biomass by fermentation) can be considered CO₂ neutral because the CO₂ yielded in the reaction is compensated by the CO₂ fixed by the biomass during its growth. Therefore, ESR is emerging as a cleaner alternative to generate hydrogen compared to the fossil fuels currently used. Recently, the use of microreaction technologies and catalytic membrane reactors have allowed strong process intensification, which in turn has increased the interest of ESR for feeding fuel cells in transportation and electronic applications³⁻⁶.



The reaction network associated to the ESR is complex, both from the mechanistic and the thermodynamic points of view⁷. The intermediate steps involved include a variety of reaction types (dehydration, dehydrogenation, reforming, WGS, methanation, etc.). They show different dependency relationships on reaction conditions and their promotion depends on different functionalities of the catalyst. In addition, formation of coke precursors from several of the compounds involved makes deactivation an important issue for the practical application of this process, which can be partly solved by the addition of alkaline promoters⁸⁻¹⁰. All these factors explain the need for extensive research of appropriate catalysts. Many studies have been focused on the ESR using supported nickel, cobalt and noble metal catalysts¹¹⁻¹⁵. An efficient catalyst for hydrogen production from ethanol has to dissociate the C-C bond at reasonably low temperatures, it has to maintain low the CO concentration and be stable under catalytic operation.

1
2
3 Noble metal-based catalysts perform well for ESR; they are stable and exhibit high
4 activity¹⁶⁻¹⁸. However, they are expensive and usually need high temperatures to be active.
5
6 The main reaction mechanism involves the decomposition of ethanol into a mixture of
7 hydrogen, carbon monoxide and methane (eq. 2), followed by the steam reforming of the
8 produced methane (eq. 3)¹⁹. Additionally, the water gas shift (WGS) reaction balances CO
9 and CO₂ rendering extra hydrogen amounts (eq. 4). Nickel catalysts are inexpensive and
10 follow the same reaction scheme, but they normally suffer from sintering and deactivation
11 by carbon deposition¹. In contrast, cobalt-based catalysts can operate at much lower
12 temperature levels when compared with noble metal- and nickel-based catalysts, typically
13 at 400-550°C, since they do not yield methane as an intermediate species in the reaction
14 mechanism, which can only be reformed at high temperature²⁰⁻²⁷. Over cobalt-based
15 catalysts, ethanol is first dehydrogenated into a mixture of hydrogen and acetaldehyde (eq.
16 5), and then acetaldehyde reacts with steam to yield hydrogen and carbon monoxide (eq. 6),
17 which participate in the WGS (eq. 4). Dimethyl ketone can be also formed via condensation
18 of acetaldehyde. A complete network of reactions can be found in literature^{7,17}.
19
20
21
22
23
24
25
26
27
28
29
30
31
32
33
34
35
36



37
38
39
40
41
42
43
44
45
46
47
48
49 An important advantage of conducting the ESR at lower temperature is that the WGS
50 equilibrium favors the formation of hydrogen and CO₂ at the expense of CO and water (eq.
51 4), thus maximizing the production of H₂ and reducing the volume of the WGS units
52 normally implemented downstream the reformer. However, most cobalt catalysts also
53
54
55
56
57
58
59
60

1
2
3 suffer from severe deactivation during ESR due to extensive carbon deposition^{11–13,28–30},
4
5 particularly under realistic loads of ethanol. The coke formation on the catalyst surface has
6
7 been related to the presence of metallic Co sites that would act as nucleation points for its
8
9 growth but there still is controversy among different reports. Essential for this matter is the
10
11 understanding of the role of the cobalt oxidation state.
12
13

14
15 In a pioneering study by *in situ* magnetic measurements, it was first demonstrated that
16
17 metallic cobalt is a very active species for the reforming of ethanol³¹. A Co/ZnO catalyst
18
19 showed 92% of reduced cobalt under ESR conditions, mainly as small superparamagnetic
20
21 nanoparticles. However, on the same catalyst, *in situ* FTIR with CO as a probe molecule
22
23 revealed that, in addition to metallic cobalt, oxidized Co species were also present at the
24
25 surface, thus suggesting that the redox pair $\text{Co}^0 \rightleftharpoons \text{Co}^{\delta+}$ is responsible for the activity of
26
27 cobalt in ESR³². Since then, the exact role of Co^0 and $\text{Co}^{\delta+}$ during ESR has been
28
29 investigated over several cobalt-based catalysts with a variety of *in situ* and *operando*
30
31 techniques with great success, and it has been recognized that the oxidation state of Co
32
33 depends on many different factors like the catalyst structure, particle size, support material
34
35 and composition of the gas phase in the reaction environment, among others^{33–42}. In
36
37 particular, considerable efforts have been addressed towards the Co/CeO₂ system due to the
38
39 large oxygen storage capacity and high oxygen mobility exhibited by ceria that prevent
40
41 extensive carbon deposition during ESR. It has been reported that proper metal-support
42
43 interaction allows only partial reduction of cobalt and leads to a superior catalytic
44
45 performance for the production of hydrogen. Specifically, $\text{Co}^{\delta+}$ with O adatoms supplied by
46
47 a reducible support facilitates the oxidative dehydrogenation of ethoxide to acetaldehyde,
48
49 while the reduced Co^0 subsequently decomposes the acetaldehyde to reforming products⁴³.
50
51
52
53
54
55
56
57
58
59
60

1
2
3 However, inconsistent results regarding the role of the oxidized cobalt species have been
4 presented for non-reducible supports. Over Al₂O₃ a balanced Co⁰:Co^{δ+} ratio of about 3:1
5 has been reported to be optimum for stable ESR performance³⁹, but over MgO it has been
6 suggested that Co^{δ+} should be minimized to avoid methanation activity⁴⁴. To conclude,
7 results have highlighted the importance of the oxidation state of cobalt in determining the
8 activity, selectivity and stability of cobalt-based catalysts for ESR, but no conclusion has
9 been made regarding the different inorganic oxide supports and their interactions with
10 cobalt, which calls for more investigations upon the active sites in working cobalt catalysts
11 under ESR conditions. Therefore, the study of the cobalt oxidation state of Co-based
12 catalysts under *in situ* and *operando* conditions is crucial to evaluate the catalyst behavior
13 under more realistic ESR conditions and can offer new insights regarding its role in the
14 activation/deactivation phenomena.
15
16
17
18
19
20
21
22
23
24
25
26
27
28
29
30

31 The aim of this work is the study of Co-spinel, Co-hydrotalcite (shortened Co-HT from
32 now on) and Co-talc in bulk and at the surface employing *in situ* X-ray Absorption Near
33 Edge Structure (XANES), *in situ* Extended X-ray absorption fine structure (EXAFS) and
34 Near Ambient Pressure X-ray Photoemission Spectroscopy (NAP-XPS), in order to
35 understand the behavior of these catalysts under ESR conditions. Co-spinel (Co₃O₄) has
36 been selected as a standard material whereas Co-talc (Co₃[Si₂O₅]₂(OH)₂) and Co-HT
37 ([Co₂Mg₄Al₂(OH)₁₆]CO₃·4H₂O) have been chosen due to their radically different catalytic
38 performance in ESR. Over Co-talc and Co-spinel, metallic Co nanoparticles are formed
39 easily under ESR conditions at 400°C, which rapidly detach from the catalyst support and
40 originate carbon nanotubes, nanofibers and platelets. The carbon deposition rate measured
41 at S/C=3 is ca. 30 mg_{carbon} g_{catalyst}⁻¹ h⁻¹ for both, Co-spinel and Co-talc⁴⁵. At the same time,
42
43
44
45
46
47
48
49
50
51
52
53
54
55
56
57
58
59
60

1
2
3 selectivity to methane and higher hydrocarbons increases at the expense of the reforming
4 products (H_2 and CO_x)^{46,47}. In contrast, the catalyst derived from Co-HT shows an excellent
5 performance for ESR at 550°C (H_2 yield of 92%) and no metallic cobalt is apparently
6 formed⁴⁸. In this case, the carbon deposition rate measured at S/C=2 is only about $1 \text{ mg}_{\text{carbon}}$
7 $\text{g}_{\text{catalyst}}^{-1} \text{ h}^{-1}$ ⁴⁸. This interesting result allows designing cobalt-based catalysts for ESR
8 without coke deposition by placing in appropriate environments $\text{Co}^{\delta+}$ active species. Long-
9 term catalytic tests (300 h) under high loads of ethanol and commercial bioethanol have
10 shown stable operation over hydrotalcite-derived cobalt catalysts without carbon deposition
11
12
13
14
15
16
17
18
19
20
21
22
23
24
25
26
27
28
29
30
31
32
33
34
35
36
37
38
39
40
41
42
43
44
45
46
47
48
49
50
51
52
53
54
55
56
57
58
59
60

2. MATERIALS AND METHODS

2.1. Catalyst preparation

Co-spinel, Co_3O_4 , was prepared by the citrate method from $\text{Co}(\text{NO}_3)_2 \cdot 6\text{H}_2\text{O}$ and citric acid as it has been previously described⁵¹. Co-talc, $\text{Co}_3[\text{Si}_2\text{O}_5]_2(\text{OH})_2$, was obtained by following the procedure described in the literature⁴⁷. Co-HT, $[\text{Co}_2\text{Mg}_4\text{Al}_2(\text{OH})_{16}]\text{CO}_3 \cdot 4\text{H}_2\text{O}$, was prepared by co-precipitation at constant pH (10 ± 0.2) by adding an aqueous solution of $\text{NaOH}/\text{Na}_2\text{CO}_3$ (2 M) onto an aqueous solution of $\text{CoCl}_2 \cdot 6\text{H}_2\text{O}$, $\text{Mg}(\text{NO}_3)_2 \cdot 6\text{H}_2\text{O}$ and $\text{Al}(\text{NO}_3)_3 \cdot 9\text{H}_2\text{O}$. The slurry was aged at 25°C for 15 h under vigorous stirring and the resulting precipitate was thoroughly washed to eliminate any Na residue and calcined at 823 for 3 h⁴⁹. The resulting material was constituted by a mixture of CoAl spinel and CoO strongly interacting with MgO, as reported in literature⁴⁸.

2.2. Characterization techniques

2.2.1. *X-ray absorption near edge structure (XANES)*

XANES measurements at Co K edge (7709 eV) were performed in quick-EXAFS transmission mode at the CLAEISS beamline⁵² of the ALBA Synchrotron Light Source. The synchrotron radiation emitted by a multi-pole wiggler was first collimated vertically by a first mirror and then monochromatised with a liquid nitrogen cooled Si (111) double crystal. The monochromatised X-ray beam was then focused down to the sample at about 800 μm x 500 μm (H x V) by changing the radius of curvature of a vertically focusing mirror. The higher harmonics contribution to desired energies was minimized by appropriately setting the rejection angles of the two mirrors in the optical hutch. The incoming and outgoing photon fluxes were measured by ionization chambers filled with an appropriate mixture of N₂ and Kr gases. Beamline energy was calibrated on the edge position of a Cobalt foil. The ethanol and water mixture for the ESR was prepared in a bubbler using He as a carrier gas in order to have an ethanol:water ratio of 1:6 in the reactor chamber (S/C=3). Reactants were introduced into the reactor chamber at atmospheric pressure and controlling the flow (20 mL/min).

2.2.2. *Extended X-ray absorption fine structure (EXAFS)*

The EXAFS data at the Co K edge were collected at CLAEISS beamline⁵² of the ALBA Synchrotron Light Source, using the same optical configuration and setup employed in the XANES experiments. EXAS data reduction has been performed according to standard procedure using DEMETER software package⁵³. For each spectrum, the raw data has been normalized by calculating and subtracting pre-edge and post-edge backgrounds as low order polynomial smooth curves. Successively the EXAFS oscillation signal has been

1
2
3 extracted. The useful k-range available for the EXAFS analysis was between 2.8 \AA^{-1} and
4
5 12.5 \AA^{-1} . A sine window has been used to truncate the EXAFS signal and a k-square
6
7 weighted Fourier transformed (FT) of it was used for visualization of the real space
8
9 distribution of Co local structure.
10
11
12
13

14 **2.2.3. Near ambient pressure X-ray photoemission spectroscopy (NAP-XPS)**

15
16
17 The X-ray photoemission spectra were recorded at the NAPP branch from CIRCE, an
18
19 undulator beamline with a photon energy range 100-2000 eV at the ALBA Synchrotron
20
21 Light Source⁵⁴. The acquisition was performed using a PHOIBOS 150 NAP electron
22
23 energy analyzer (SPECS GmbH) equipped with four differential pumping stages and a set
24
25 of electrostatic lenses which enable to perform XPS measurements with the sample at
26
27 pressures from ultra-high vacuum (UHV, with a base pressure of $2-5 \times 10^{-10}$ mbar) and up
28
29 to 20 mbar. The take-off angle was approximately 50° and the angle between the analyzer
30
31 axis and the incoming synchrotron radiation horizontal linear polarization vector was 54.7° ,
32
33 the magic angle. The spectra were acquired with 20 μm exit slit and the diameter of the X-
34
35 ray spot was estimated to be in the order of $100 \mu\text{m} \times 65 \mu\text{m}$ (H x V). Two different photon
36
37 energies were used: 965 and 1250 eV, to provide variable surface sensitivity, *i.e.* the
38
39 inelastic mean free paths (IMFP) were close to 0.5 and 0.9 nm respectively⁵⁵. The spectra
40
41 were acquired with 20 eV pass energy with an overall (analyzer and monochromator)
42
43 energy resolution lower than 300 meV full width at half-maximum (FWHM): 276 meV for
44
45 $h\nu = 965 \text{ eV}$ and 291 meV for 1250 eV. For the data analysis, the spectra were calibrated
46
47 with respect to C1s (at a binding energy of 284.7 eV) and fitted by Gaussian/Lorentzian
48
49 convolution functions using the CASAXPS software. The background was modeled by a
50
51
52
53
54
55
56
57
58
59
60

1
2
3 Shirley background function. The ethanol and water mixture for the ESR was prepared in a
4 bubbler like for the XANES experiments, but using Ar as carrier gas, in order to maintain
5 an ethanol:water ratio of 1:6 in the analysis chamber (S/C=3). Reactants were introduced
6 into the analysis chamber by means of a leak valve. Another leak valve was used to feed
7 H₂. The NAP-XPS experiments were performed at a sample pressure of 0.1 mbar. The
8 samples were mounted on a stainless steel plate and were heated using an infrared laser
9 with $\lambda=808$ nm. The sample temperature was monitored with a K-type thermocouple in
10 direct contact with the samples.
11
12
13
14
15
16
17
18
19
20
21
22
23

24 **3. RESULTS AND DISCUSSION**

25 **3.1. *In situ* XANES**

26
27 The K-edge X-ray Absorption Near Edge Structure (XANES) of cobalt has been often
28 used to characterize the bulk of Co-based materials due to the possibility of detecting
29 spectral changes in the near edge features related to the local structural and electronic
30 properties of the compounds. These spectral variations appear as resonances characterized
31 by different energy positions and/or intensities in the pre-peak and absorption edge⁵⁶.
32
33 Figure 1 shows the evolution of the Co K-edge XANES spectra of the three different Co-
34 based materials studied, *i.e.* Co₃O₄, Co-talc and Co-HT, under ESR reaction conditions.
35
36 Additionally, the spectra of five different cobalt compounds are presented in the bottom of
37 the plot to be used as references: (a) LiCoO₂, (b) Co₃O₄, (c) CoO, (d) Co(OH)₂ and (e)
38 metallic Co foil. When increasing the sample temperature from room temperature (RT) to
39 550°C under ESR reaction conditions, Co K-edge XANES reveals significant changes in
40 the cobalt electronic structure which indicate a reduction process for all the samples
41
42
43
44
45
46
47
48
49
50
51
52
53
54
55
56
57
58
59
60

1
2
3 studied. The spinel phase Co_3O_4 exhibits a mixture of Co oxidation states where two thirds
4 from the total Co ions correspond to trivalent cations in octahedral positions while one third
5 corresponds to divalent cations occupying tetrahedral sites^{51,57}. No significant changes are
6 observed in the pre-edge features when heating from 250°C up to 400°C and only partial
7 reduction to CoO is detected at temperatures around 400°C, but above 500°C, the formation
8 of metallic cobalt phase masks the contribution of the cations (Figure 1). For the Co-talc
9 system there are not clear spectral changes up to 500°C and from this temperature to 550°C,
10 the spectral features reveal that part of the cobalt is reduced to metallic phase, as shown in
11 Figure 1, where a clear shoulder at ca. 7709 eV assigned to metallic cobalt appears.
12 However, a different behavior is observed for the Co-HT system. In this case, like for the
13 Co_3O_4 reference sample, there is a partial reduction to Co(II) already detected at 300°C but
14 there is no further reduction to metallic Co at higher temperatures. The final state for the
15 Co-HT is characterized by an increase of the intensity of the white line and the resonance
16 transitions and multiple scattering contributions seem to correspond to a combination of
17 CoO and $\text{Co}(\text{OH})_2$ phases. Nevertheless, some features like the pre-edge and oscillations
18 intensities are not fully reproduced by linear combination. Unlike in the other studied
19 samples, the pre-edge peak for the Co-HT remains with the same shape even at 550°C (see
20 Figure 1) and there is no indication of reduction to metallic Co. In fact, the Co-HT sample
21 has been previously calcined and its thermal decomposition yields a well dispersed mixture
22 of CoAl spinels⁵⁰, which is similar to cobalt spinels, but cobalt is in a more complex
23 environment surrounded by other oxide phases (MgO , Al_2O_3)⁴⁸.
24
25
26
27
28
29
30
31
32
33
34
35
36
37
38
39
40
41
42
43
44
45
46
47
48
49
50
51
52
53
54
55
56
57
58
59
60

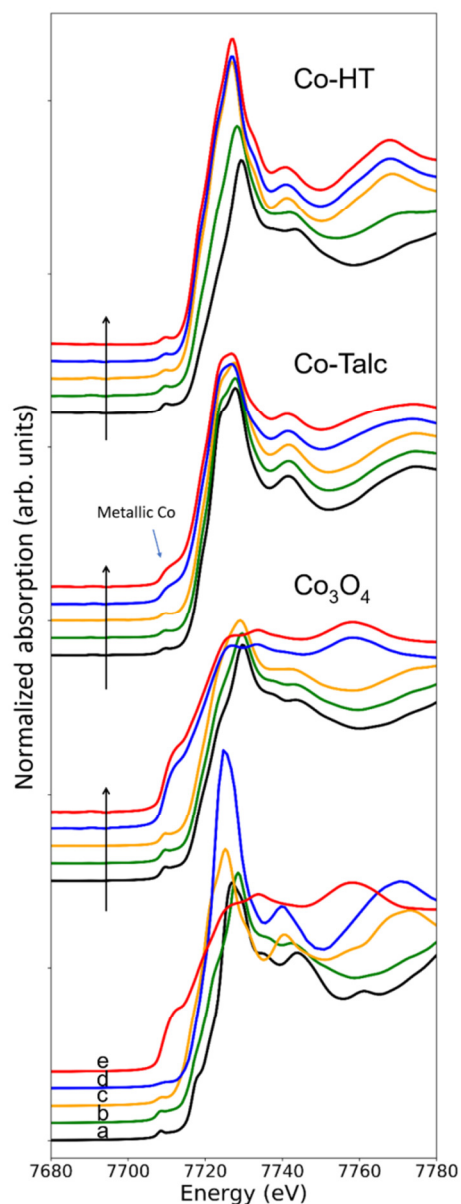


Figure 1. *In situ* Co K-edge XANES during ESR reaction at different temperatures for the three tested catalysts: Co₃O₄, Co-talc and Co-HT. The spectra for each temperature are displayed with different colors: 250 (black), 300 (green), 400 (orange), 500 (blue) and 550°C (red). In the bottom the spectra for five reference compounds are plotted (all at room temperature): (a) LiCoO₂ (black), (b) Co₃O₄ (green), (c) CoO (orange), (d) Co(OH)₂ (blue) and (e) Co foil (red).

1
2
3
4
5 The similarities in the spectral features for different chemical environments and the
6 complexity of the reduction pathway in samples such as Co-talc and Co-HT could lead to
7 misinterpretation of the experimental results. However, the cobalt average oxidation state
8 can be easily estimated considering the energy edge shift in our samples and other standard
9 cobalt compounds and using integral methods as described by Capehart *et. al.*⁵⁸. This
10 approach has been already applied in order to follow the reduction process of Co in bulk
11 materials⁵⁹. Figure 2a shows the calibration curve obtained using metallic Co, CoO, Co₃O₄
12 and LiCoO₂ as reference compounds and employing this integral method (a more detailed
13 description of its application can be found in the supplementary information). In this way it
14 is possible to get the evolution of the average oxidation state of the samples studied under
15 ESR conditions and different temperatures (Figure 2b). Co₃O₄ shows a slight decrease of
16 the average oxidation state from 250°C to 400°C which correlates to the partial formation of
17 CoO described from the spectra evolution in Figure 1, but from 400°C to 500°C a dramatic
18 reduction to metallic state is observed. The average charge of Co ions in the Co-talc sample
19 at 250°C is close to 2.1 ± 0.2 probably due to different local environments and strong
20 interactions within the silicate matrix that would also explain the different spectral features
21 observed with respect to the CoO reference sample. Then, when increasing the temperature
22 to 500°C, the Co oxidation state decreases down to 1.4 ± 0.2 , which indicates the partial
23 reduction to metallic Co and therefore the presence of a mixture of chemical phases as
24 shown in the near edge features (Figure 1). On the other hand, Co-HT exhibits an oxidation
25 state close to 3 at 250°C which smoothly decreases one unit at 400°C and no further
26 reduction is observed at higher temperatures. For this sample there are no insights of
27 metallic Co formation as stated when discussing the XANES spectra.
28
29
30
31
32
33
34
35
36
37
38
39
40
41
42
43
44
45
46
47
48
49
50
51
52
53
54
55
56
57
58
59
60

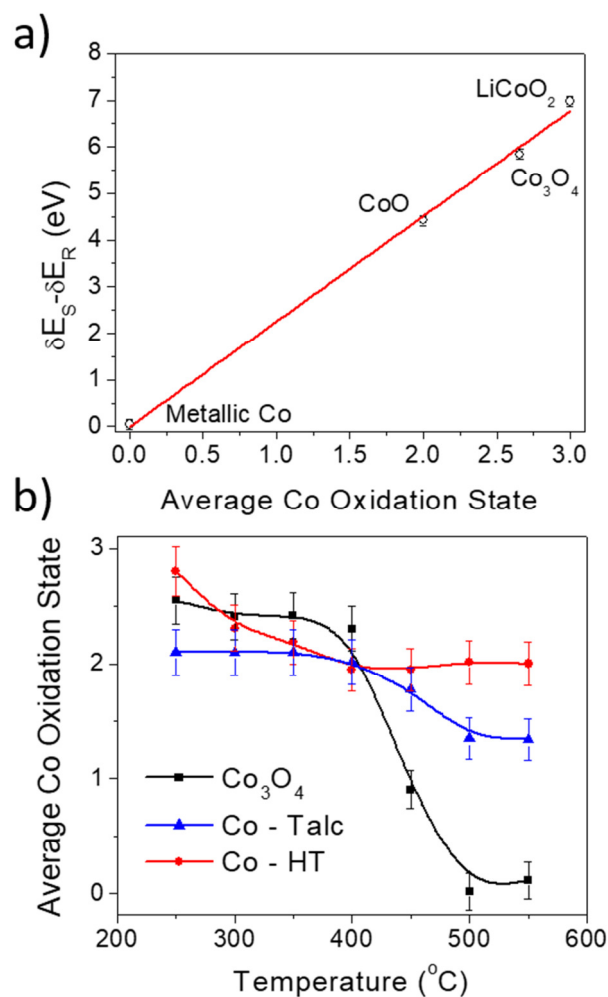


Figure 2. (a) Calibration curve employing different oxide references. These values have been calculated using integral methods as described by Capehart *et. al.*⁵⁸ (see supplementary information). The curve slope was 2.26 ± 0.08 with $R^2 = 0.996$. (b) Average oxidation state of the bulk material under ESR reaction conditions as a function of temperature.

More detailed information has been obtained for Co_3O_4 , Co-talc and Co-HT systems through chemical speciation by linear combination of XANES references. Co_3O_4 , CoO and metallic Co were employed to analyze the Co_3O_4 reduction under ESR conditions (Figure

1
2
3 3a). The references used to analyze the behavior of Co-talc under ESR conditions were Co-
4 talc (the same sample measured at room temperature under He atmosphere), CoO and
5 metallic Co (Figure 3b) while the selected references to analyze the chemical changes of
6 Co-HT were the original Co-HT, CoO and Co-HT after H₂ reduction (named as Reduced
7 Co-HT), as illustrated in Figure 3c. The selection of these references was based on the
8 similarities of their spectral features with the ones shown by the samples studied at different
9 temperatures. For both samples, Co₃O₄ and Co-talc, the cobalt reduction to the metallic
10 form is through a Co(II) intermediate (most likely CoO). For Co₃O₄ the formation of
11 metallic Co at 500°C is already close to 100% (Figure 3a). On the other hand, for Co-talc,
12 previous crystallographic measurements reported for similar nanocomposites revealed that
13 phase segregation takes place through delamination of the talc nanolayers under ESR
14 reaction conditions⁴⁷. Figure 3b shows that Co-talc treated at 550°C still has around 32% of
15 the cobalt inside the matrix, 40% as CoO and 28% as metallic Co. From the results at this
16 temperature, the average oxidation state calculated for Co is 1.47 ± 0.06 (this value depends
17 on the formal charge assigned to the Co in the Co-talc, in this case considered as +2.1)
18 which is in agreement with the value obtained by the integral method. Co-HT, initially with
19 an average oxidation state of approximately +2.8 (named as Co-HT in Figure 3c), yields
20 Reduced Co-HT (as named in Figure 3c) with an average oxidation state close to +2 even
21 below 400°C. In this case, it was not possible to complete the spectral fitting with only
22 these two contributions (Co-HT and Reduced Co-HT) and a third component was required
23 in order to improve the linear fit. The features for the third contribution were very similar to
24 the CoO phase and this contribution was more important at high temperatures than near
25 400°C. Although it has been remarked the complexity in which different phases can coexist
26
27
28
29
30
31
32
33
34
35
36
37
38
39
40
41
42
43
44
45
46
47
48
49
50
51
52
53
54
55
56
57
58
59
60

in this sample under different conditions, this assumption worked well for explaining the reduction behavior in a simple way.

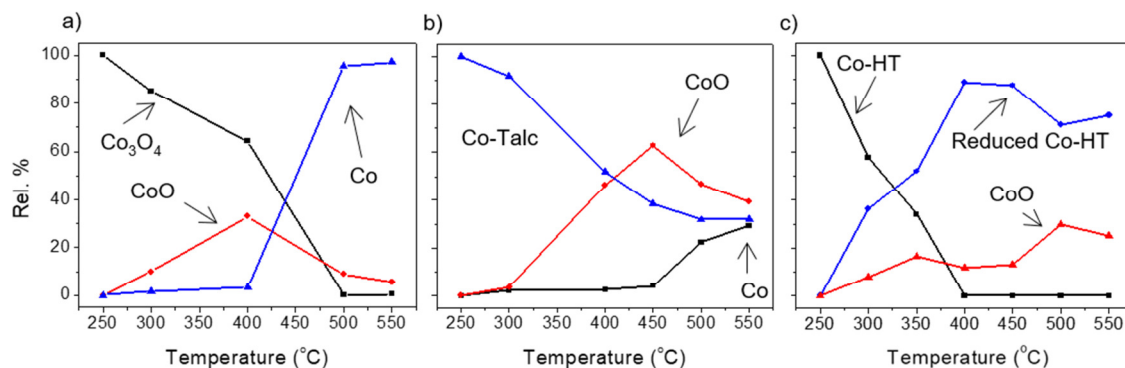


Figure 3. Relative component composition for (a) Co_3O_4 , (b) Co-talc and (c) Co-HT samples under ESR reaction conditions as a function of temperature (R^2 is higher than 0.996 in all cases).

3.2. *In situ* EXAFS

Figure 4a shows the raw EXAFS data acquired *in situ* under ESR reaction conditions and different temperatures for Co_3O_4 and Figure 4b their corresponding Fourier Transform (FT). Following the results of the linear combination analysis of the XANES, and comparing to the reference spectra, the Co_3O_4 pure fraction progressively decreases in favor of CoO and metallic Co. Coherently the EXAFS signals can be analyzed as a combination of these three phases. The analysis of the other samples, Co-talc and Co-HT is complex due to the multiple phases present. Under similar reaction conditions than for Co_3O_4 , the raw EXAFS data and the corresponding FT for Co-talc and Co-HT are shown in Figure 5a,b and Figure 6a,b respectively. In a similar way than Co_3O_4 , Co-talc EXAFS signals change significantly during reaction and, in agreement with the results of the linear

combination analysis of the XANES, the Co-talc fraction also progressively decreases in favor of CoO and metallic Co, but to a lesser extent than the Co_3O_4 sample. Nevertheless, unlike Co_3O_4 and Co-talc, Co-HT EXAFS signals don't change significantly during the ESR reaction at different temperatures, which again is in agreement with the XANES results exposed above and supports the no formation of metallic Co for this sample.

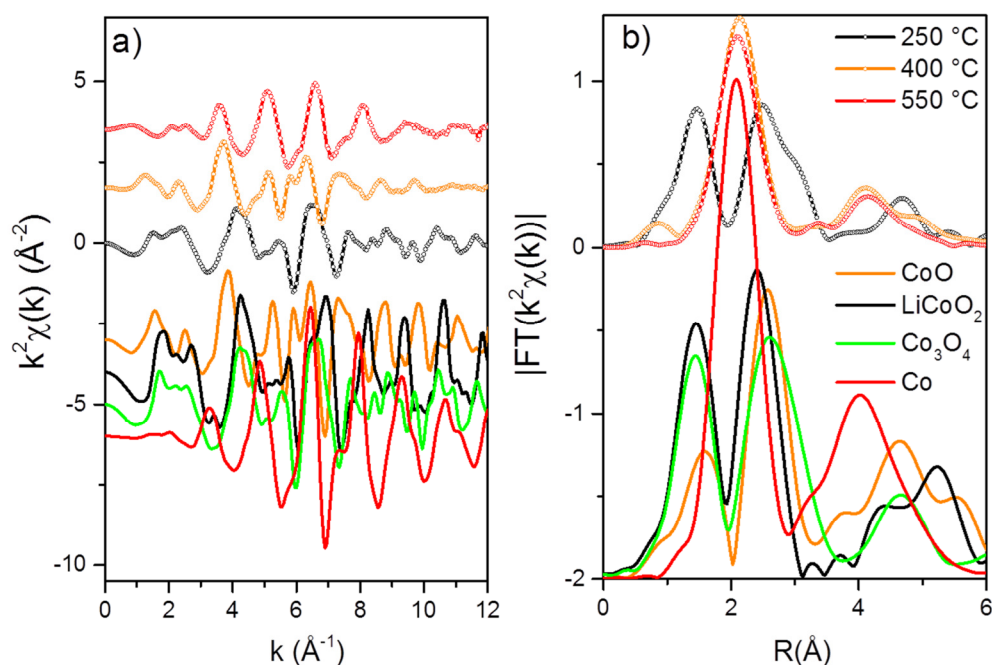


Figure 4. (a) Raw EXAFS data for the Co_3O_4 sample under ESR reaction conditions and at increasing temperatures. (b) Corresponding Fourier Transformations. The spectra for each temperature are displayed with different colors: 250 (black), 400 (orange) and 550°C (red). In the bottom the spectra for four reference compounds are plotted (all at room temperature): LiCoO_2 (black), Co_3O_4 (green), CoO (orange) and (e) Co foil (red).

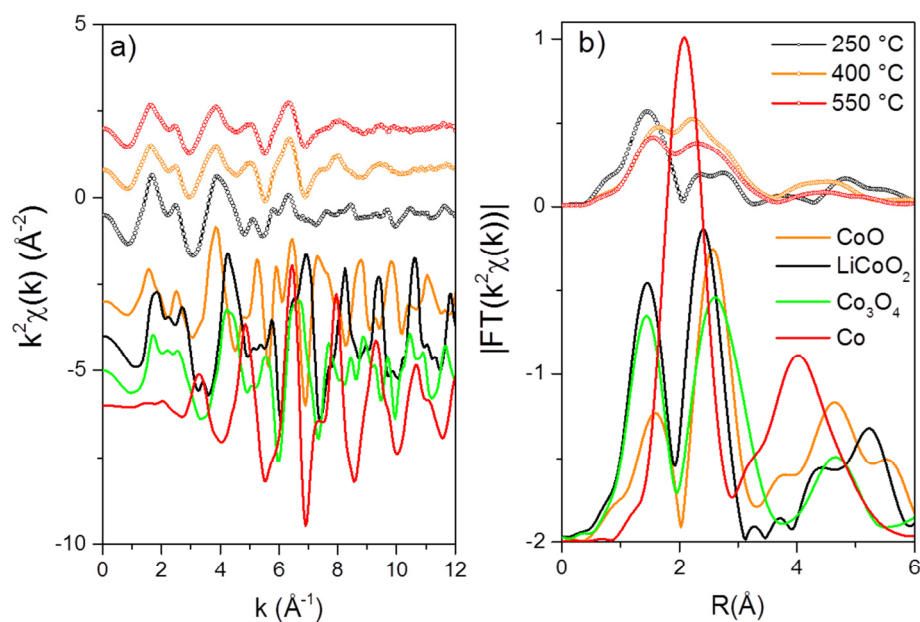


Figure 5. (a) Raw EXAFS data for the Co-talc sample under ESR reaction conditions and at increasing temperatures. (b) Corresponding Fourier Transformations. The spectra for each temperature are displayed with different colors: 250 (black), 400 (orange) and 550°C (red). In the bottom the spectra for four reference compounds are plotted (all at room temperature): LiCoO_2 (black), Co_3O_4 (green), CoO (orange) and (e) Co foil (red).

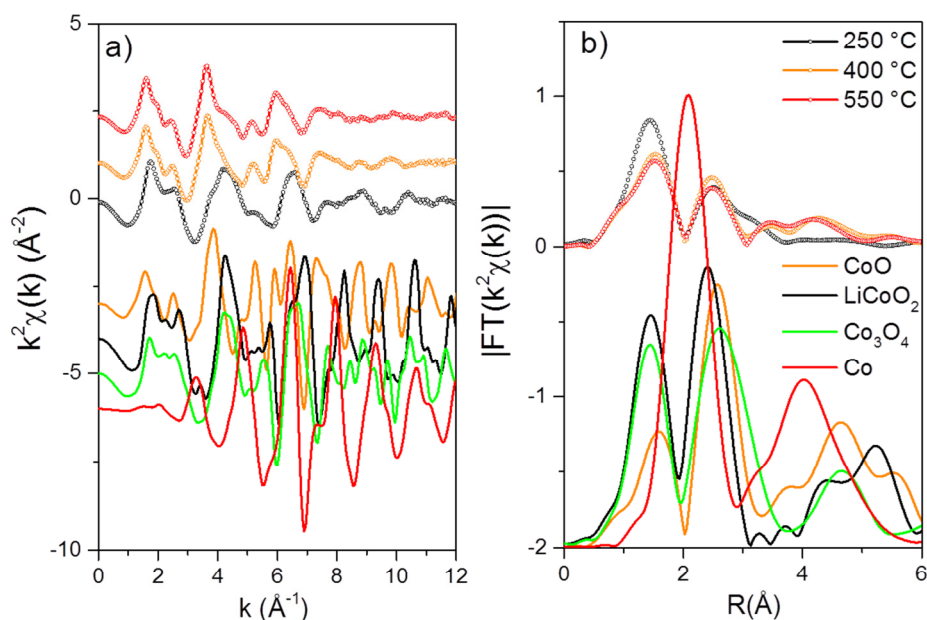


Figure 6. Raw EXAFS data for the Co-HT sample under ESR reaction conditions and at increasing temperatures. (b) Corresponding Fourier Transformations. The spectra for each temperature are displayed with different colors: 250 (black), 400 (orange) and 550°C (red). In the bottom the spectra for four reference compounds are plotted (all at room temperature): LiCoO₂ (black), Co₃O₄ (green), CoO (orange) and (e) Co foil (red).

3.3. *In situ* Near Ambient Pressure XPS (NAP-XPS)

The surface and subsurface regions constitute the active part of the catalyst in catalytic heterogeneous reactions since it is the part that interacts with the reactant gases. X-ray Photoemission Spectroscopy (XPS) is a technique traditionally used under high vacuum conditions that allows studying the composition and electronic structure of surfaces. Since

1
2
3 the results from experiments performed *ex situ* under vacuum conditions can differ from
4 those obtained under more realistic environments, XPS, among other techniques, has been
5 further improved in order to break or diminish the so-called pressure gap⁶⁰. In the case of
6 XPS, the implementation of a differentially pumping system and a set of electrostatic lenses
7 have enabled to work at near ambient pressures with good statistics⁶¹⁻⁶³. The possibility of
8 studying samples under different gas mixtures has proved that the surface composition
9 directly depends on the reaction environment, among other factors, pointing out the need to
10 measure under *operando* or *in situ* conditions^{18,64}.

21 *In situ* NAP-XPS measurements were done in order to study the chemical state and local
22 environment of cobalt during the ESR reaction thus providing information about its surface
23 chemistry and complement the bulk information obtained by XANES. In order to
24 understand the catalysts behavior under the ethanol/water reaction atmosphere used for
25 ESR reaction, where H₂ is generated creating a local reducing environment, the catalysts
26 were also exposed in a separate experiment (with a different pellet made from the same
27 sample) to pure H₂ to compare the final state for both experimental conditions. For all the
28 samples, spectra were acquired under *in situ* conditions at 0.1 mbar and room temperature,
29 and then the temperature was increased while the pressure was kept constant.

41 The C 1s signal did not show significant changes under ESR reaction conditions (Figure
42 S5) for all the samples studied. Taking into account the amount of carbon deposition
43 measured in our previous catalytic tests⁴⁵⁻⁴⁸, longer reaction times are required to follow the
44 evolution of the C 1s signal, which was not possible due to beamtime limitation.

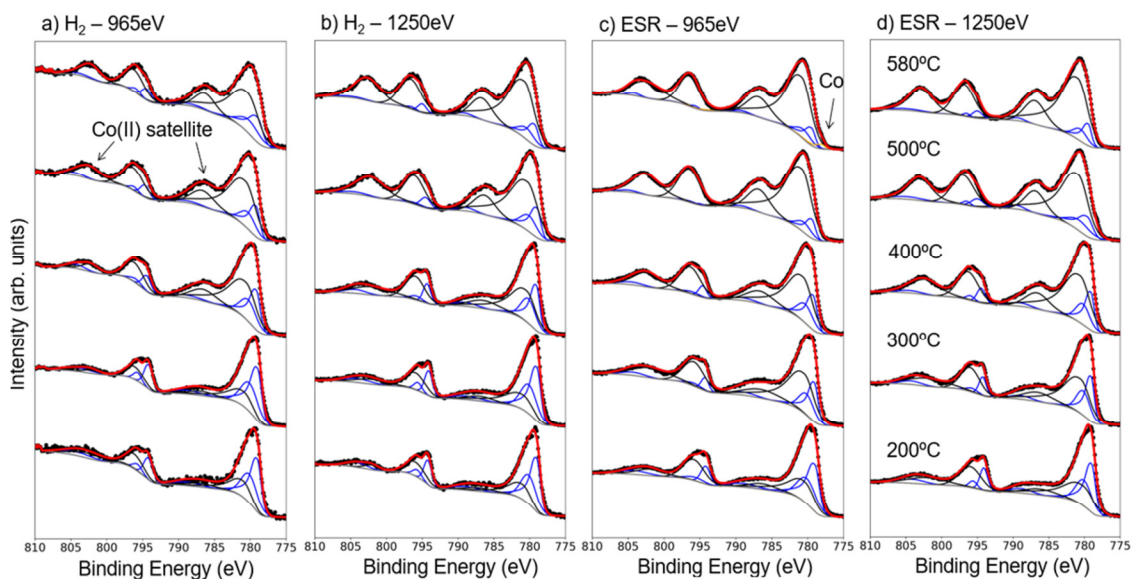
51 The interpretation of Co XP spectra is not straightforward due to peak asymmetries,
52 binding energy (BE) overlap of the metallic and oxide species and their satellites, the
53 different complex environments present in Co-talc and Co-HT samples and the charging

1
2
3 effects. In order to minimize the uncertainty and error in the peak assignment process, the
4 data treatment has been done according to the procedure reported by Biesinger *et. al.*⁶⁵
5 which describes in detail the curve fitting procedure for various chemical states of Co-
6 containing samples. Following this reference, only the more intense components and its
7 satellites have been considered in a more simplified way to facilitate the interpretation of
8 the results. In spite of the complications to measure non-conductive samples like Co-talc, or
9 samples exhibiting complex environments, like Co-talc and Co-HT, a clear evolution is
10 observed in all cases, as illustrated below.

21 22 23 **3.3.1. Co_3O_4**

24
25
26 Figure 7 shows the XP spectra of Co_3O_4 under H_2 (Figure 7a,b) and ESR conditions
27 (Figure 7c,d) with two different incident photon energies to provide information at different
28 depths: 965 eV (Figure 7a,c) and 1250 eV (Figure 7b,d). There is a common trend in both
29 gas environments, a progressive reduction of Co_3O_4 when heating. At 200°C, the spectra
30 under ESR mixture and H_2 show the typical shape for the Co_3O_4 cubic normal spinel
31 structure, which exhibits one third of tetrahedrally coordinated Co^{2+} and two thirds of
32 octahedrally coordinated Co^{3+} . Nevertheless, at the highest temperature tested (580°C) the
33 samples are reduced to CoO (or hydroxide), and metallic cobalt traces are detected during
34 ESR conditions but not under H_2 atmosphere. The peak associated to the main Co $2p_{3/2}$
35 component of Co_3O_4 (779.6 eV) is sharper and at slightly lower energy than the one
36 corresponding to CoO (780.0 eV and similar values for the hydroxide species)⁶⁵. Besides,
37 Co_3O_4 exhibits a weak shake-up satellite at higher binding energies (around 10 eV from the
38 main peak) while CoO has a characteristic strong satellite at 786 eV (around 6eV above the
39 main peak). This strong satellite observed in the CoO photoemission is explained by the
40
41
42
43
44
45
46
47
48
49
50
51
52
53
54
55
56
57
58
59
60

1
2
3 octahedrally coordinated, high-spin Co^{2+} oxides, where charge is transferred from the
4 ligand to the 3d orbital enabling different final states in the photoemission process. Instead,
5
6 ligand to the 3d orbital enabling different final states in the photoemission process. Instead,
7
8 for Co_3O_4 the satellite peak is weaker because the two thirds of octahedrally coordinated
9
10 Co^{3+} states do not contribute to charge transfer and only the remaining one third
11
12 tetrahedrally coordinated Co^{2+} give rise to shake-up peaks^{66,67}.
13
14
15
16
17



18
19
20
21
22
23
24
25
26
27
28
29
30
31
32
33
34
35
36
37
38 **Figure 7.** *In situ* near ambient pressure Co $2p_{3/2}$ XPS for Co_3O_4 exposed to H_2 (a,b) and
39 ESR atmosphere (c,d). The experiments were carried out at different temperatures as
40 indicated in the right panel and with two different photon incidence energies: 965eV (a,c)
41 and 1250 eV (b,d). Co_3O_4 : blue lines, CoO : black lines, metallic Co in orange, in grey the
42 background and in red the envelope.
43
44
45
46
47
48
49
50
51
52

53 The evolution of the surface relative composition (Co_3O_4 vs CoO) under a particular gas
54 environment with the temperature (Figure 8) does not show significant differences at
55
56
57
58
59
60

different penetration depths, only a slight surface oxidation under ESR conditions at 200°C that disappears progressively when increasing the temperature. However, comparing the evolution under H₂ with respect to ESR conditions, the sample is more reduced when exposed to ESR reaction conditions under the temperature range tested. These results indicate that at the temperatures at which the material is active for hydrogen production the ESR environment is more reducing than pure H₂. Even at lower temperatures, where the dehydrogenation of ethanol takes place, the sample is overall more reduced under ESR. It is worth noting that traces of metallic Co are detected at 580°C using 965 eV incidence energy (this was confirmed by increasing the temperature to 660°C, see Figure S2 in supporting information) while this metallic phase is not observed under H₂ gas.

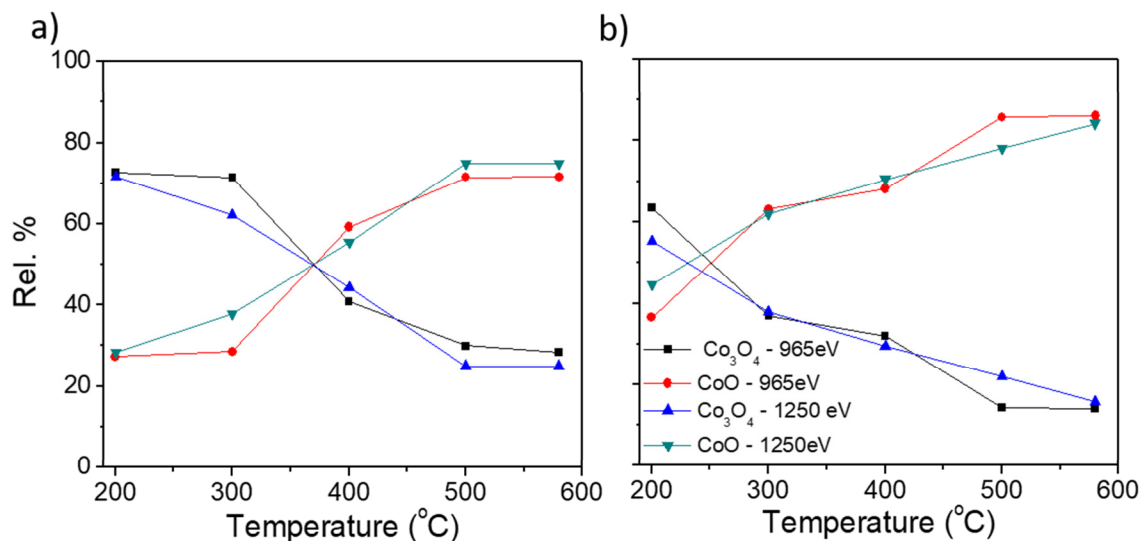


Figure 8. Relative surface composition (Co₃O₄ vs CoO) as a function of temperature and penetration depth for: (a) pure H₂, and (b) ESR reaction mixture.

1
2
3 Figure 9 shows the O1s spectra of Co_3O_4 obtained with 965 eV photon energy, therefore
4 displaying the most surface sensitive results. The spectra are composed by the contributions
5 from the oxygen lattices of Co_3O_4 and CoO but the energy separation between the O1s peak
6 of both oxides is less than 0.2 eV and it is not possible to resolve them (both with a BE
7 close to ~ 530 eV). Other contributions to the O1s signal arise from hydroxide or hydrated
8 oxide species, around ~ 531.5 eV, and from surface bonded water or organic alcohols
9 around 532.5 eV⁶⁵. At 200°C the reduction of cobalt by pure H_2 produces water that
10 hydrates the surface and about 40% of the total O1s total area correspond to adsorbed H_2O
11 and hydroxide species while ESR promotes hydroxide formation increasing this percentage
12 to 60%. When the temperature is increased to 580°C, these contributions decay to 13-14%
13 both under H_2 and ESR gas environments and the spectra obtained are equivalent (Figure
14 9).
15
16
17
18
19
20
21
22
23
24
25
26
27
28
29
30
31
32
33
34
35
36
37
38
39
40
41
42
43
44
45
46
47
48
49
50
51
52
53
54
55
56
57
58
59
60

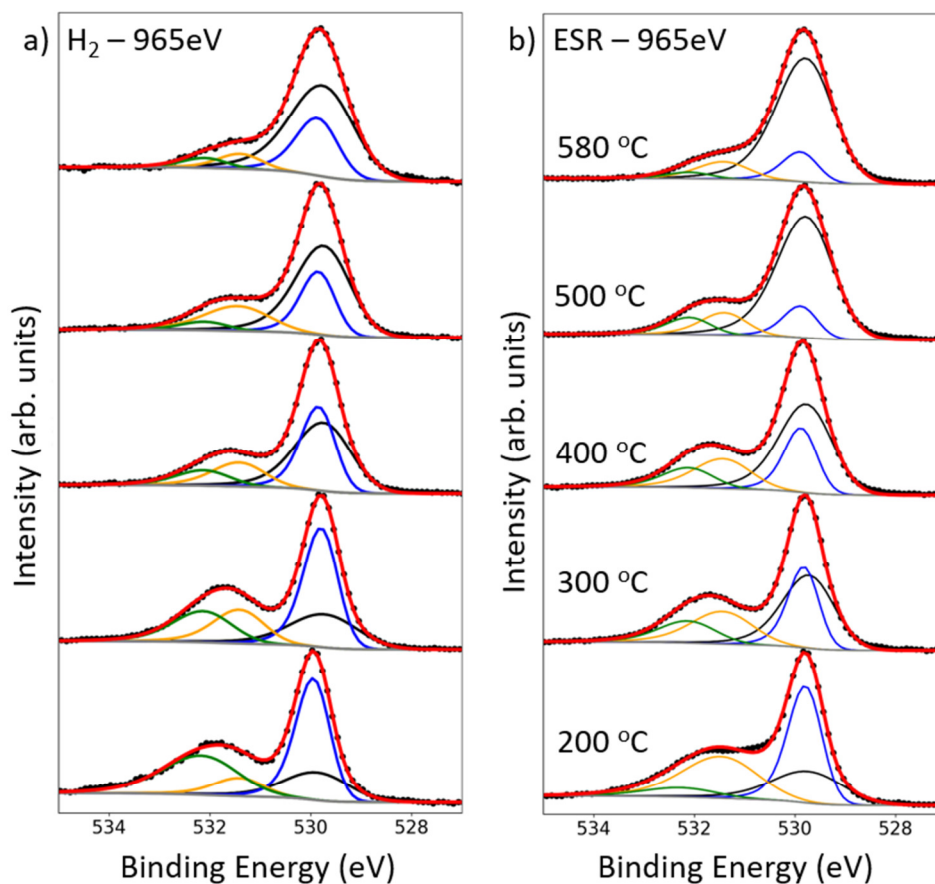


Figure 9. *In situ* near ambient pressure O1s XPS (acquired with 965 eV photon energy) of Co_3O_4 exposed to: (a) H_2 , and (b) ESR atmosphere. The experiments were carried out at different temperatures as indicated in the right panel. The contribution of water or alcohol bounded to the surface region is displayed in green and the contribution of the hydroxide (or hydrated) oxide in orange. The black line represents the Co_3O_4 contribution and the blue line the CoO. The weight of each compound was estimated by the Co $2p_{3/2}$ fitting procedure described before⁶⁵.

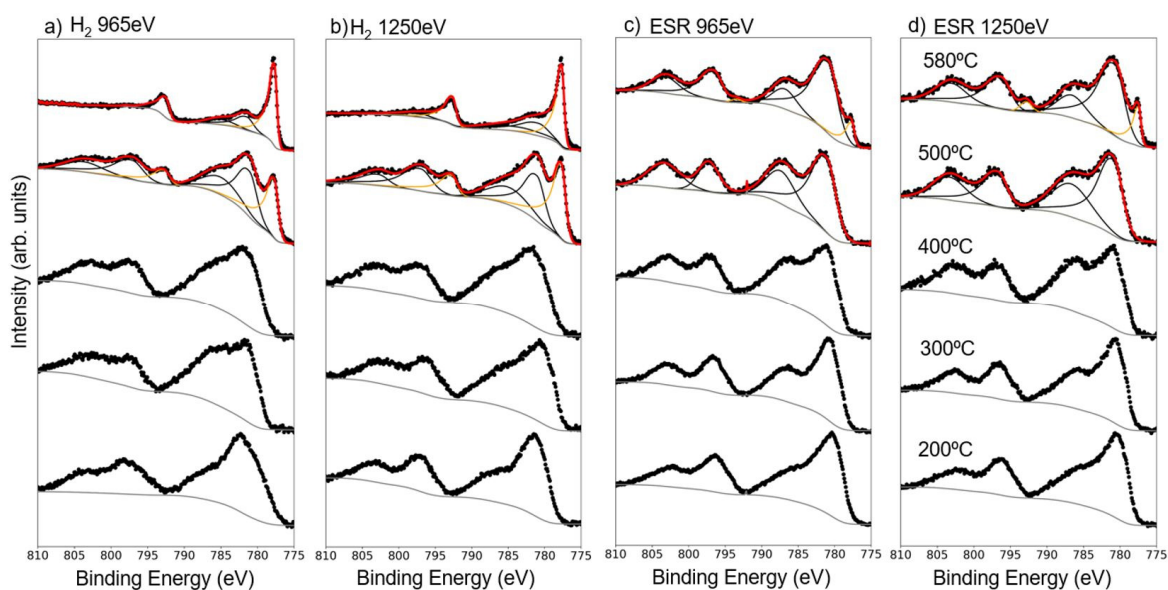
3.3.2. Co-talc

1
2
3 In the Co-talc sample, the cobalt ions are embedded in a complex matrix formed by the
4 talc structure and this fact justifies the broad peaks and satellites obtained for Co 2p spectra
5 (Figure 10). Under both gas environments studied, at lower temperatures (200°C) - unlike
6 Co₃O₄ - there is already a clear satellite which indicates that most of the cobalt corresponds
7 to high spin Co(II), which is in agreement with the structure of the Co-talc, where the metal
8 occupies octahedral sites with a Co²⁺ oxidation state. However, the peaks are broad due to
9 charging and to the presence of different local environments of the Co atoms within the talc
10 matrix. When heating under H₂ gas there are changes in the spectra that could be ascribed
11 to Co reorganization or migration up to 400°C, but it is difficult to assign different
12 components. In this case it can only be noted a clear evolution to metallic Co at higher
13 temperatures (500 - 580°C).
14
15
16
17
18
19
20
21
22
23
24
25
26
27

28 Under ESR reaction conditions and high temperatures (400 - 500°C) there is a phase
29 segregation process between the talc sheets and CoO (which exhibits a sharper satellite)
30 and then at 580°C CoO is partially reduced to metallic cobalt, as illustrated in Figure 10c,d.
31 Preliminary transmission electron microscopy studies on similar Co-talc catalysts exposed
32 to ESR reaction conditions (*ex situ*) revealed the partial formation of metallic Co NP of 3
33 nm size⁴⁷. This CoO phase transition is not so easily detected under H₂. In this case the
34 reduction to metallic Co at 580°C is not partial as observed for ESR conditions, but almost
35 complete. Furthermore, it is worth noting that the metallic Co contribution is larger at
36 higher photon energies (bigger penetration length) for both reactive environments. It has
37 been reported that the formation of a very stable 3 to 5 nm thick CoO phase takes place
38 during redox reactions of Co NPs by a complex mechanism which can inhibit the reaction
39 path to metallic nanoparticles (or reoxidize them into Co₃O₄)⁶⁸. The reduction of cobalt
40 under H₂ gas involves cation migration and metallic NP formation, while under ESR
41
42
43
44
45
46
47
48
49
50
51
52
53
54
55
56
57
58
59
60

1
2
3 reaction conditions, *in situ* XPS suggests the formation of a CoO phase before reduction
4
5 which could partially hamper the evolution to metallic Co.
6
7
8
9

10 As previously mentioned, in the case of the Co_3O_4 sample metallic Co is only detected as
11 a trace under the ESR reaction conditions studied, therefore the formation of metallic Co
12 NP from the Co-talc sample exposed to the same experimental conditions could be
13 NP from the Co-talc sample exposed to the same experimental conditions could be
14 explained through a combination of surface energy and mechanical tension due to the
15 silicate layers confinement. While for the Co_3O_4 sample the reduction degree is higher
16 under ESR conditions than under H_2 atmosphere; for the Co-talc sample the measurements
17 under H_2 result in a higher reduction degree as compared to ESR reaction conditions. In
18 addition, the high water partial pressure in the ESR atmosphere could also hinder the
19 formation of SiO_2 , which is formed during the reduction of the Co-talc structure.
20
21
22
23
24
25
26
27
28
29
30
31
32
33
34
35
36
37



1
2
3 **Figure 10.** *In situ* near ambient pressure Co 2p_{3/2} XPS for Co-talc exposed to H₂ (a,b) and
4
5 ESR atmosphere (c,d) The experiments were carried out at different temperature as
6
7 indicated in the right panel and with two different photon incidence energies: 965eV (a,c)
8
9 and 1250 eV (b,d). Co⁺²: black lines, metallic Co: orange lines. In grey the background and
10
11 in red line the envelope.
12
13
14
15
16
17

18 3.3.3. Co-HT

19
20 Figure 11 shows the analysis of the XP Co 2p spectra for the Co-HT sample acquired
21
22 with two different photon energies under H₂ gas (Figure 11a,b) and ESR conditions (Figure
23
24 11c,d). In all cases there is a clear reduction from Co(III) to Co(II) indicated by a
25
26 remarkable increase of the satellite attributed to high spin Co(II) between 500°C and 580°C,
27
28 but there is no evidence of metallic Co in all the experimental conditions tested. Three
29
30 contributions were used in order to fit the experimental data: a Co(III) contribution at low
31
32 energies (~779 eV); a low spin Co(II) from spinel structure at ~780 eV with a small
33
34 satellite 9.5-10eV shifted respected from the main peak; and finally, a high spin Co(II) like
35
36 CoO oxide with a 2p_{3/2} transition at ~781eV with a satellite with 6eV difference respected
37
38 from the main peak.
39
40
41
42

43 Above 500°C there are no significant differences between the spectra obtained under both
44
45 reaction conditions except for the width of the Co 2p peaks, which are larger when
46
47 measuring under pure H₂. The thermal treatment in H₂ reducing media could lead to
48
49 CoAl₂O₄ formation, which exhibits around 1 eV shift of the Co 2p to higher energies with
50
51 respect to the CoO contribution⁶⁹. Instead, in ESR atmosphere the Co 2p peaks are
52
53 narrower and this fact could be attributed to a thin CoO or Co(OH)₂ surface layer, which
54
55
56
57
58
59
60

should be more active for hydrogen production than CoAl_2O_4 ³⁴. The presence of MgO could lead to complex dehydrogenation and dehydration routes depending on the temperature conditions⁷⁰, and the generated by-products along with the presence of water could produce a partial segregation of the cobalt oxide from the main matrix. XP spectra of the Al 2p and Mg 2s regions did not change significantly during the experiments and they are assigned to their respective oxides (data not shown).

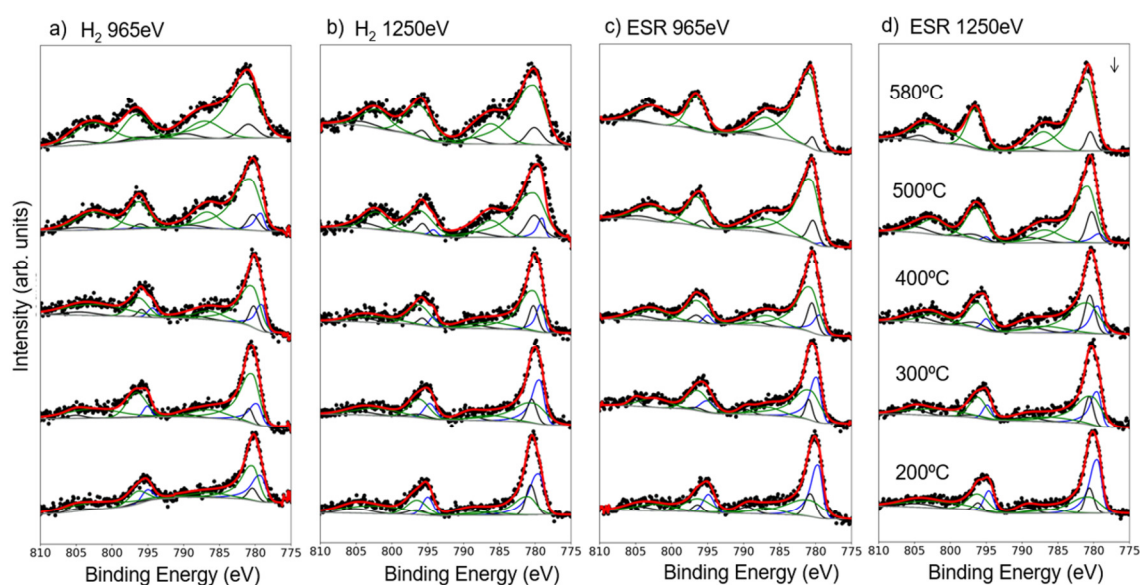


Figure 11. *In situ* near ambient pressure Co $2p_{3/2}$ XPS of Co-HT exposed to H_2 (a,b) and ESR atmosphere (c,d). The experiments were carried out at different temperatures as indicated in the right panel and with two different photon energies: 965eV (a,c) and 1250 eV (b,d). Co^{2+} in tetrahedral environments: black lines, high spin Co^{2+} in octahedral positions: green lines, Co^{3+} : blue lines. In grey the background and in red line the envelope.

4. CONCLUSIONS

1
2
3 In this work, two different Co-based catalysts, Co-talc and Co-HT, have been studied by
4 *in situ* XANES, EXAFS and NAP-XPS under ESR conditions. Moreover, Co₃O₄ spinel has
5
6 been studied as reference with the same techniques. Both, XANES and NAP-XPS, are
7
8 complementary since they probe the bulk or surface of the materials studied respectively.
9
10 On the one hand, XANES results from bulk analysis show that while for the standard
11
12 Co₃O₄ sample there is a complete reduction to metallic Co under ESR at more than 500°C,
13
14 under the same conditions Co-talc is only partially reduced to metallic Co and Co-HT does
15
16 not exhibit metallic Co at all. The Co-HT shows a complex environment with the
17
18 coexistence of different phases and during the ESR reaction at increasing temperatures the
19
20 Co is only partially reduced from +2.8 to +2. On the other hand, NAP-XPS measurements
21
22 have been carried out to study the most superficial layers of these Co-based catalysts
23
24 interacting with ESR and H₂ gas environments at different temperatures. For Co₃O₄ there is
25
26 a partial reduction of the initial spinel phase to CoO under both gases by increasing the
27
28 temperature. In this case, at the highest temperature and at the lowest excitation energy, *i.e.*
29
30 the most surface sensitive, metallic Co traces are detected during ESR but not under H₂.
31
32 This would imply a more reducing environment under ESR (which generates H₂ locally)
33
34 than H₂. Compiling the results from both techniques and considering the unavoidable
35
36 pressure gap (XANES experiments are performed at atmospheric pressure while NAP-XPS
37
38 experiments are restricted to the mbar pressure range) we could infer that metallic Co will
39
40 be formed under realistic ESR pressure conditions. Furthermore, it must be considered that
41
42 the reduction of CoO produces water which must segregate from the inner layers towards
43
44 the material surface. For the case of Co-talc, the obtained NAP-XPS results show a partial
45
46 reduction to metallic Co, as observed with XANES, which could be attributed to the
47
48 segregation of metallic Co NPs. This also agrees with previous publications reporting the
49
50
51
52
53
54
55
56
57
58
59
60

1
2
3 formation of Co metallic nanoparticles under ESR reaction conditions. In this case, the
4
5 formation of metallic Co is higher in the case of H₂ gas as compared to ESR and this could
6
7 be explained by the formation of a CoO layer in the latter case which may partially obstruct
8
9 the obtention of Co⁰. Finally, the Co-HT sample does not show any indication of metallic
10
11 Co by NAP-XPS under any of the environments tested, corroborating the XANES results.
12
13 The evolution with temperature of the XP spectra under H₂ and ESR show a partial
14
15 reduction from Co(III) to Co(II) as indicated by the increase of the satellite attributed to
16
17 high spin Co(II). Our experimental findings support the hypothesis that correlates the
18
19 deactivation of Co catalysts under ESR reaction conditions with the nucleation and growth
20
21 of carbon on metallic Co sites. For Co-spinel and Co-talc it has been previously described
22
23 how carbon nanostructures cover the catalyst surface decreasing their performance, but Co-
24
25 HT has demonstrated an excellent behavior and long-term stability under ESR conditions.
26
27 The results shown in this work confirm that there is no metallic Co formation for Co-HT
28
29 under *in situ* ESR emphasizing the importance of designing Co catalysts with Co^{δ+} active
30
31 species under appropriate environments that hinder the formation of metallic Co in order to
32
33 avoid deactivation by carbon deposition.
34
35
36
37
38
39
40
41

42 **Supporting information**

43
44
45 Estimation of Cobalt average oxidation state from XANES measurements by applying the
46
47 method reported by Capehart *et. al.* Supplementary *in situ* Near Ambient Pressure X-ray
48
49 Photoemission measurements of Co-spinel, Co-talc and Co-HT (PDF).
50
51
52
53
54
55
56
57
58
59
60

Author Contributions

The manuscript was written through contributions of all authors. All authors have given approval to the final version of the manuscript.

Funding Sources

Argentinian National Research Council (CONICET)

Departament d'Innovació, Universitats i Empresa, Generalitat de Catalunya (GC 2017 SGR 128)

Ministerio de Economía y Competitividad / FEDER (ENE2015-63969-R)

Acknowledgements

C.H.-I. acknowledges the Argentinian National Research Council (CONICET) for the financial support (He is also a member of the research staff of CONICET). JL is a Serra Húnter Fellow and is grateful to ICREA Academia program and grants MINECO/FEDER ENE2015-63969-R and GC 2017 SGR 128. The authors would like to thank the support of ALBA staff for the successful performance of the measurements at CIRCE and CLAESS beamlines from the ALBA Synchrotron Light Source.

References

- (1) Li, D.; Li, X.; Gong, J. Catalytic Reforming of Oxygenates: State of the Art and Future Prospects. *Chem. Rev.* 2016, 116, 11529–11653.
- (2) Llorca, J.; Cortés, V.; Divins, N. J.; Olivera, R.; E., T. Hydrogen from Bioethanol. In *Renewable Hydrogen Technologies*; Gandía, L. M., Arzamendi, G., Diéguez, P. M., Eds.; Elsevier, 2013; p. 135–169.
- (3) Llorca, J.; Casanovas, A.; Trifonov, T.; Rodríguez, A.; Alcubilla, R. First use of macroporous silicon loaded with catalyst film for a chemical reaction: A microreformer for producing hydrogen from ethanol steam reforming. *J. Catal.* 2008, 255, 228–233.
- (4) Divins, N. J.; López, E.; Rodríguez, Á.; Vega, D.; Llorca, J. Bio-ethanol steam reforming and autothermal reforming in 3- μm channels coated with RhPd/CeO₂ for hydrogen generation. *Chem. Eng. Process. Process Intensif.* 2013, 64, 31–37.
- (5) Pla, D.; Salleras, M.; Morata, A.; Garbayo, I.; Gerbolés, M.; Sabaté, N.; Divins, N. J.; Casanovas, A.; Llorca, J.; Tarancón, A. Standalone ethanol micro-reformer integrated on silicon technology for onboard production of hydrogen-rich gas. *Lab Chip* 2016, 16, 2900–2910.
- (6) Koch, R.; López, E.; Divins, N. J.; Allué, M.; Jossen, A.; Riera, J.; Llorca, J. Ethanol catalytic membrane reformer for direct PEM FC feeding. *Int. J. Hydrogen Energy* 2013, 38, 5605–5615.

- 1
2
3 (7) Song, H.; Zhang, L.; Ozkan, U. S. Investigation of the Reaction Network in Ethanol
4 Steam Reforming over Supported Cobalt Catalysts. *Ind. Eng. Chem. Res.* 2010, 2,
5 8984–8989.
6
7
8
9
10 (8) Llorca, J.; Homs, N.; Sales, J.; Fierro, J. L. G.; De La Piscina, P. R. Effect of sodium
11 addition on the performance of Co-ZnO-based catalysts for hydrogen production
12 from bioethanol. *J. Catal.* 2004, 222, 470–480.
13
14
15
16
17 (9) Kim, K. S.; Seo, H. R.; Lee, S. Y.; Ahn, J. G.; Shin, W. C.; Lee, Y. K. TPR and
18 EXAFS studies on Na-promoted Co/ZnO catalysts for ethanol steam reforming. *Top.*
19 *Catal.* 2010, 53, 615–620.
20
21
22
23
24
25 (10) Sharma, Y. C.; Kumar, A.; Prasad, R.; Upadhyay, S. N. Ethanol steam reforming for
26 hydrogen production: Latest and effective catalyst modification strategies to
27 minimize carbonaceous deactivation. *Renew. Sustain. Energy Rev.* 2017, 74, 89–103.
28
29
30
31
32
33 (11) Vaidya, P. D.; Rodrigues, A. E. Insight into steam reforming of ethanol to produce
34 hydrogen for fuel cells. *Chem. Eng. J.* 2006, 117, 39–49.
35
36
37
38 (12) Haryanto, A.; Fernando, S.; Murali, N.; Adhikari, S. Current Status of Hydrogen
39 Production Techniques by Steam Reforming of Ethanol: A Review. *Energy & Fuels*
40 2005, 19, 2098–2106.
41
42
43
44
45 (13) Ni, M.; Leung, D. Y. C.; Leung, M. K. H. A review on reforming bio-ethanol for
46 hydrogen production. *Int. J. Hydrogen Energy* 2007, 32, 3238–3247.
47
48
49
50
51 (14) Contreras, J. L.; Salmones, J.; Colín-Luna, J. A.; Nuño, L.; Quintana, B.; Córdova,
52 I.; Zeifert, B.; Tapia, C.; Fuentes, G. A. Catalysts for H₂ production using the ethanol
53
54
55
56
57
58
59
60

- 1
2
3 steam reforming (a review). *Int. J. Hydrogen Energy* 2014, 39, 18835–18853.
4
5
6 (15) Hou, T.; Zhang, S.; Chen, Y.; Wang, D.; Cai, W. Hydrogen production from ethanol
7 reforming: Catalysts and reaction mechanism. *Renew. Sustain. Energy Rev.* 2015, 44,
8 132–148.
9
10
11 (16) Deluga, G. A.; Salge, J. R.; Schmidt, L. D.; Verykios, X. E. Renewable Hydrogen
12 from Ethanol by Autothermal Reforming. *Science* 2004, 303, 993–997.
13
14
15 (17) Zanchet, D.; Santos, J. B. O.; Damyanova, S.; Gallo, J. M. R.; Bueno, J. M. C.
16 Toward understanding metal-catalyzed ethanol reforming. *ACS Catal.* 2015, 5,
17 3841–3863.
18
19
20 (18) Divins, N. J.; Angurell, I.; Escudero, C.; Pérez-Dieste, V.; Llorca, J. Influence of the
21 support on surface rearrangements of bimetallic nanoparticles in real catalysts.
22 *Science* 2014, 346, 620–623.
23
24
25
26
27 (19) Idriss, H.; Scott, M.; Llorca, J.; Chan, S. C.; Chiu, W.; Sheng, P.-Y.; Yee, A.;
28 Blackford, M. A.; Pas, S. J.; Hill, A. J.; Alamgir F.M.; Rettew R.; Petersburg C.;
29 Senanayake S. D.; Barteau M.A. A phenomenological study of the metal-oxide
30 interface: the role of catalysis in hydrogen production from renewable resources.
31 *ChemSusChem* 2008, 1, 905–910.
32
33
34
35 (20) Llorca, J.; Homs, N.; Sales, J.; Ramírez de la Piscina, P. Efficient Production of
36 Hydrogen over Supported Cobalt Catalysts from Ethanol Steam Reforming. *J. Catal.*
37 2002, 209, 306–317.
38
39
40
41
42
43
44
45
46
47
48
49
50
51
52
53
54
55 (21) Mariño, F.; Baronetti, G.; Jobbagy, M.; Laborde, M. Cu-Ni-K/ γ -Al₂O₃ supported
56
57
58
59
60

- 1
2
3 catalysts for ethanol steam reforming: Formation of hydrotalcite-type compounds as
4 a result of metal-support interaction. *Appl. Catal. A Gen.* 2003, 238, 41–54.
5
6
7
8
9 (22) Llorca, J.; Ramírez De La Piscina, P.; Dalmon, J. A.; Sales, J.; Homs, N. Co-free
10 hydrogen from steam-reforming of bioethanol over ZnO-supported cobalt catalysts:
11 Effect of the metallic precursor. *Appl. Catal. B Environ.* 2003, 43, 355–369.
12
13
14
15
16 (23) Batista, M. S.; Santos, R. K. .; Assaf, E. M.; Assaf, J. M.; Ticianelli, E. A. High
17 efficiency steam reforming of ethanol by cobalt-based catalysts. *J. Power Sources*
18 2004, 134, 27–32.
19
20
21
22
23
24 (24) Vargas, J. C.; Libs, S.; Roger, A.-C.; Kiennemann, A. Study of Ce-Zr-Co fluorite-
25 type oxide as catalysts for hydrogen production by steam reforming of bioethanol.
26 *Catal. Today* 2005, 107–108, 417–425.
27
28
29
30
31
32 (25) Frusteri, F.; Freni, S. Bio-ethanol, a suitable fuel to produce hydrogen for a molten
33 carbonate fuel cell. *J. Power Sources* 2007, 173, 200–209.
34
35
36
37 (26) Song, H.; Ozkan, U. S. Ethanol steam reforming over Co-based catalysts: Role of
38 oxygen mobility. *J. Catal.* 2009, 261, 66–74.
39
40
41
42
43 (27) Sohn, H.; Ozkan, U. S. Cobalt-Based Catalysts for Ethanol Steam Reforming: An
44 Overview. *Energy and Fuels* 2016, 30, 5309–5322.
45
46
47
48 (28) Vicente, J.; Montero, C.; Ereña, J.; Azkoiti, M. J.; Bilbao, J.; Gayubo, A. G. Coke
49 deactivation of Ni and Co catalysts in ethanol steam reforming at mild temperatures
50 in a fluidized bed reactor. *Int. J. Hydrogen Energy* 2014, 39, 12586–12596.
51
52
53
54
55
56 (29) Chiou, J. Y. Z.; Lai, C. L.; Yu, S. W.; Huang, H. H.; Chuang, C. L.; Wang, C. Bin.
57
58
59
60

- 1
2
3 Effect of Co, Fe and Rh addition on coke deposition over Ni/Ce_{0.5}Zr_{0.5}O₂ catalysts
4 for steam reforming of ethanol. *Int. J. Hydrogen Energy* 2014, 39, 20689–20699.
5
6
7
8
9 (30) Iulianelli, A.; Palma, V.; Bagnato, G.; Ruocco, C.; Huang, Y.; Veziroğlu, N. T.;
10 Basile, A. From bioethanol exploitation to high grade hydrogen generation: Steam
11 reforming promoted by a Co-Pt catalyst in a Pd-based membrane reactor. *Renew.*
12 *Energy* 2018, 119, 834–843.
13
14
15
16
17
18 (31) Llorca, J.; Dalmon, J. A.; Ramírez De la Piscina, P.; Homs, N. In situ magnetic
19 characterisation of supported cobalt catalysts under steam-reforming of ethanol.
20 *Appl. Catal. A Gen.* 2003, 243, 261–269.
21
22
23
24
25
26 (32) Llorca, J.; Homs, N.; Ramírez de la Piscina, P. In situ DRIFT-mass spectrometry
27 study of the ethanol steam-reforming reaction over carbonyl-derived Co/ZnO
28 catalysts. *J. Catal.* 2004, 227, 556–560.
29
30
31
32
33
34 (33) Turczyniak, S.; Luo, W.; Papaefthimiou, V.; Ramgir, N. S.; Haevecker, M.;
35 MacHocki, A.; Zafeiratos, S. A Comparative Ambient Pressure X-ray Photoelectron
36 and Absorption Spectroscopy Study of Various Cobalt-Based Catalysts in Reactive
37 Atmospheres. *Top. Catal.* 2016, 59, 532–542.
38
39
40
41
42
43
44 (34) de Lima, A. E. P.; de Oliveira, D. C. In situ XANES study of Cobalt in Co-Ce-Al
45 catalyst applied to Steam Reforming of Ethanol reaction. *Catal. Today* 2017, 283,
46 104–109.
47
48
49
50
51
52 (35) Sohn, H.; Soykal, I. I.; Zhang, S.; Shan, J.; Tao, F.; Miller, J. T.; Ozkan, U. S. Effect
53 of cobalt on reduction characteristics of ceria under ethanol steam reforming
54
55
56
57
58
59
60

- 1
2
3 conditions: AP-XPS and XANES studies. *J. Phys. Chem. C* 2016, 120, 14631–
4
5 14642.
6
7
8
9 (36) Turczyniak, S.; Greluk, M.; Słowik, G.; Gac, W.; Zafeiratos, S.; Machocki, A.
10 Surface State and Catalytic Performance of Ceria-Supported Cobalt Catalysts in the
11 Steam Reforming of Ethanol. *ChemCatChem* 2017, 9, 782–797.
12
13
14
15
16 (37) Bayram, B.; Soykal, I. I.; Von Deak, D.; Miller, J. T.; Ozkan, U. S. Ethanol steam
17 reforming over Co-based catalysts: Investigation of cobalt coordination environment
18 under reaction conditions. *J. Catal.* 2011, 284, 77–89.
19
20
21
22
23
24 (38) Turczyniak, S.; Teschner, D.; Machocki, A.; Zafeiratos, S. Effect of the surface state
25 on the catalytic performance of a Co/CeO₂ ethanol steam-reforming catalyst. *J.*
26 *Catal.* 2016, 340, 321–330.
27
28
29
30
31
32 (39) Passos, A. R.; Martins, L.; Pulcinelli, S. H.; Santilli, C. V.; Briois, V. Effect of the
33 balance between Co(II) and Co(0) oxidation states on the catalytic activity of cobalt
34 catalysts for Ethanol Steam Reforming. *Catal. Today* 2014, 229, 88–94.
35
36
37
38
39 (40) Óvári, L.; Krick Calderon, S.; Lykhach, Y.; Libuda, J.; Erdohelyi, A.; Papp, C.; Kiss,
40 J.; Steinrück, H. P. Near ambient pressure XPS investigation of the interaction of
41 ethanol with Co/CeO₂(111). *J. Catal.* 2013, 307, 132–139.
42
43
44
45
46
47 (41) Ávila-Neto, C. N.; Liberatori, J. W. C.; Da Silva, A. M.; Zanchet, D.; Hori, C. E.;
48 Noronha, F. B.; Bueno, J. M. C. Understanding the stability of Co-supported
49 catalysts during ethanol reforming as addressed by in situ temperature and spatial
50 resolved XAFS analysis. *J. Catal.* 2012, 287, 124–137.
51
52
53
54
55
56
57
58
59
60

- 1
2
3 (42) Kim, K. S.; Lee, Y. K. The active phase of NaCo/ZnO catalyst for ethanol steam
4 reforming: EXAFS and in situ XANES studies. *Int. J. Hydrogen Energy* 2010, 35,
5 5378–5382.
6
7
8
9
10 (43) Martono, E.; Hyman, M. P.; Vohs, J. M. Reaction pathways for ethanol on model
11 Co/ZnO(0001) catalysts. *Phys. Chem. Chem. Phys.* 2011, 13, 9880–9886.
12
13
14
15 (44) Karim, A. M.; Su, Y.; Engelhard, M. H.; King, D. L.; Wang, Y. Catalytic Roles of
16 Co^0 and Co^{2+} during Steam Reforming of Ethanol on Co/MgO Catalysts. *ACS Catal.*
17 2011, 1, 279–286.
18
19
20
21
22
23 (45) Domínguez, M.; Cristiano, G.; López, E.; Llorca, J. Ethanol steam reforming over
24 cobalt talc in a plate microreactor. *Chem. Eng. J.* 2011, 176, 280–285.
25
26
27
28 (46) Domínguez, M.; Taboada, E.; Molins, E.; Llorca, J. Co–SiO₂ aerogel-coated
29 catalytic walls for the generation of hydrogen. *Catal. Today* 2008, 138, 193–197.
30
31
32
33 (47) Domínguez, M.; Taboada, E.; Idriss, H.; Molins, E.; Llorca, J. Fast and efficient
34 hydrogen generation catalyzed by cobalt talc nanolayers dispersed in silica aerogel.
35 *J. Mater. Chem.* 2010, 20, 4875.
36
37
38
39 (48) Espinal, R.; Taboada, E.; Molins, E.; Chimentao, R. J.; Medina, F.; Llorca, J. Cobalt
40 hydrotalcite for the steam reforming of ethanol with scarce carbon production. *RSC*
41 *Adv.* 2012, 2, 2946–2956.
42
43
44 (49) Espinal, R.; Taboada, E.; Molins, E.; Chimentao, R. J.; Medina, F.; Llorca, J. Cobalt
45 hydrotalcites as catalysts for bioethanol steam reforming. The promoting effect of
46 potassium on catalyst activity and long-term stability. *Appl. Catal. B Environ.* 2012,
47
48
49
50
51
52
53
54
55
56
57
58
59
60

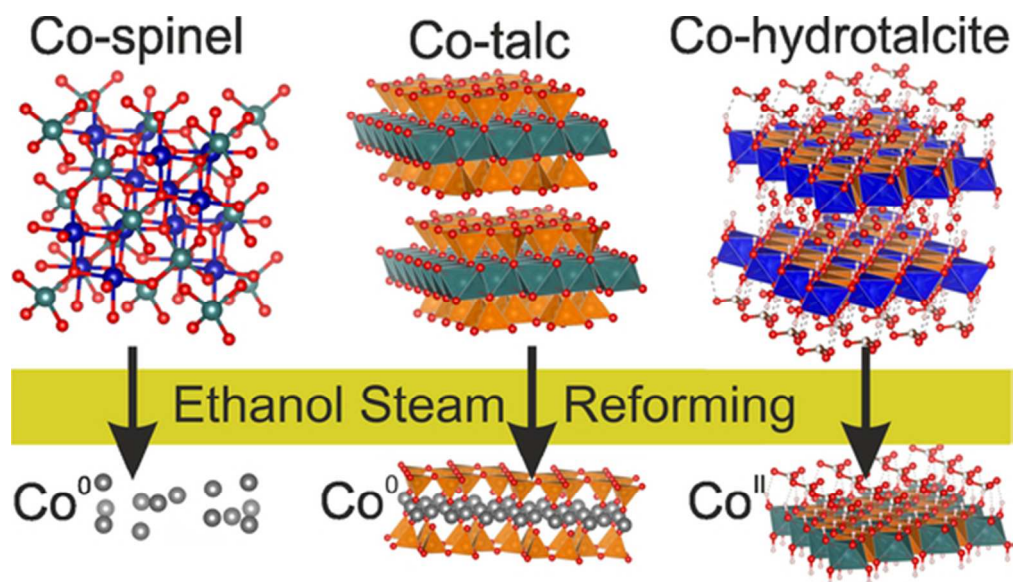
- 1
2
3 127, 59–67.
4
5
6 (50) Espinal, R.; Anzola, A.; Adrover, E.; Roig, M.; Chimentao, R.; Medina, F.; López,
7
8 E.; Borio, D.; Llorca, J. Durable ethanol steam reforming in a catalytic membrane
9
10 reactor at moderate temperature over cobalt hydrotalcite. *Int. J. Hydrogen Energy*
11
12 2014, 39, 10902–10910.
13
14
15
16 (51) Llorca, J.; Ramírez De La Piscina, P.; Dalmon, J.-A.; Homs, N. Transformation of
17
18 Co_3O_4 during ethanol steam-re-forming. Activation process for hydrogen production.
19
20 *Chem. Mater.* 2004, 16, 3573–3578.
21
22
23
24 (52) Simonelli, L.; Marini, C.; Olszewski, W.; Ávila Pérez, M.; Ramanan, N.; Guilera,
25
26 G.; Cuartero, V.; Klementiev, K. CLÆSS: The hard X-ray absorption beamline of
27
28 the ALBA CELLS synchrotron. *Cogent Phys.* 2016, 3, 1231987.
29
30
31
32 (53) Ravel, B.; Newville, M. ATHENA, ARTEMIS, HEPHAESTUS: Data analysis for
33
34 X-ray absorption spectroscopy using IFEFFIT. *J. Synchrotron Radiat.* 2005, 12,
35
36 537–541.
37
38
39 (54) Pérez-Dieste, V.; Aballe, L.; Ferrer, S.; Nicolàs, J.; Escudero, C.; Milán, A.;
40
41 Pellegrin, E. Near Ambient Pressure XPS at ALBA. *J. Phys. Conf. Ser.* 2013, 425,
42
43 072023.
44
45
46
47 (55) Powell, C. J.; Jablonski, A. *NIST Electron Inelastic-Mean-Free-Path Database,*
48
49 *version 1.2, SRD71*; National Institute of Standards and Technology, 2010.
50
51
52 (56) Jiang, T.; Ellis, D. E. X-ray absorption near edge structures in cobalt oxides. *J. Mater.*
53
54 *Res.* 1996, 11, 2242–2256.
55
56
57
58
59
60

- 1
2
3 (57) de la Peña O'Shea, V. A.; Homs, N.; Pereira, E. B.; Nafria, R.; Ramírez de la
4
5 Piscina, P. X-ray diffraction study of Co_3O_4 activation under ethanol steam-
6
7 reforming. *Catal. Today* 2007, 126, 148–152.
8
9
10 (58) Capehart, T. W.; Herbst, J. F.; Mishra, R. K.; Pinkerton, F. E. X-ray-absorption edge
11
12 shifts in rare-earth-transition-metal compounds. *Phys. Rev. B* 1995, 52, 7907–7914.
13
14
15 (59) Krylova, G.; Giovanetti, L. J.; Requejo, F. G.; Dimitrijevic, N. M.; Prakapenka, A.;
16
17 Shevchenko, E. V. Study of nucleation and growth mechanism of the metallic
18
19 nanodumbbells. *J. Am. Chem. Soc.* 2012, 134, 4384–4392.
20
21
22 (60) Escudero, C.; Salmeron, M. From solid-vacuum to solid-gas and solid-liquid
23
24 interfaces: In situ studies of structure and dynamics under relevant conditions. *Surf.*
25
26 *Sci.* 2013, 607, 2–9.
27
28
29 (61) Ogletree, D. F.; Bluhm, H.; Lebedev, G.; Fadley, C. S.; Hussain, Z.; Salmeron, M. A
30
31 differentially pumped electrostatic lens system for photoemission studies in the
32
33 millibar range. *Rev. Sci. Instrum.* 2002, 73, 3872.
34
35
36 (62) Frank Ogletree, D.; Bluhm, H.; Hebenstreit, E. D.; Salmeron, M. Photoelectron
37
38 spectroscopy under ambient pressure and temperature conditions. *Nucl. Instruments*
39
40 *Methods Phys. Res. Sect. A Accel. Spectrometers, Detect. Assoc. Equip.* 2009, 601,
41
42 151–160.
43
44
45 (63) Salmeron, M.; Schlögl, R. Ambient pressure photoelectron spectroscopy: A new tool
46
47 for surface science and nanotechnology. *Surf. Sci. Rep.* 2008, 63, 169–199.
48
49
50 (64) Tao, F.; Grass, M. E.; Zhang, Y.; Butcher, D. R.; Renzas, J. R.; Liu, Z.; Chung, J. Y.;
51
52
53
54
55
56
57
58
59
60

- 1
2
3 Mun, B. S.; Salmeron, M.; Somorjai, G. A. Reaction-Driven Restructuring of Rh-Pd
4 and Pt-Pd Core-Shell Nanoparticles. *Science* 2008, 322, 932–934.
5
6
7
8
9 (65) Biesinger, M. C.; Payne, B. P.; Grosvenor, A. P.; Lau, L. W. M.; Gerson, A. R.;
10 Smart, R. S. C. Resolving surface chemical states in XPS analysis of first row
11 transition metals, oxides and hydroxides: Cr, Mn, Fe, Co and Ni. *Appl. Surf. Sci.*
12 2011, 257, 2717–2730.
13
14
15
16
17
18 (66) Petitto, S. C.; Marsh, E. M.; Carson, G. A.; Langell, M. A. Cobalt oxide surface
19 chemistry: The interaction of CoO(100), Co₃O₄(110) and Co₃O₄(111) with oxygen
20 and water. *J. Mol. Catal. A Chem.* 2008, 281, 49–58.
21
22
23
24
25
26 (67) Vaz, C. A. F.; Prabhakaran, D.; Altman, E. I.; Henrich, V. E. Experimental study of
27 the interfacial cobalt oxide in Co₃O₄/α-Al₂O₃ (0001) epitaxial films. *Phys. Rev. B -*
28 *Condens. Matter Mater. Phys.* 2009, 80, 1–7.
29
30
31
32
33
34 (68) Papaefthimiou, V.; Dintzer, T.; Dupuis, V.; Tamion, A.; Tournus, F.; Hillion, A.;
35 Teschner, D.; Hävecker, M.; Knop-Gericke, A.; Schlögl, R.; Zafeirotos, S. Nontrivial
36 redox behavior of nanosized cobalt: New insights from ambient pressure X-ray
37 photoelectron and absorption spectroscopies. *ACS Nano* 2011, 5, 2182–2190.
38
39
40
41
42
43
44 (69) Bhattacharya, A. K.; Hartridge, A.; Mallick, K. K.; Werrett, C. R. Low-temperature
45 decomposition of hydrated transition metal chlorides on hydrous gel substrates. *J.*
46 *Mater. Sci.* 1996, 31, 4479–4482.
47
48
49
50
51
52 (70) Chieragato, A.; Ochoa, J. V.; Bandinelli, C.; Fornasari, G.; Cavani, F.; Mella, M. On
53 the chemistry of ethanol on basic oxides: Revising mechanisms and intermediates in
54
55
56
57
58
59
60

the lebedev and guerbet reactions. *ChemSusChem* 2015, 8, 377–388.





48x27mm (300 x 300 DPI)